KSME

Springer

Journal of Mechanical Science and Technology 35 (2) 2021

Original Article
DOI 10.1007/s12206-021-0130-2

Keywords:
· Drug delivery
· Electrolysis micropump
· Wireless power transfer
· Bio-MEMS

Correspondence to:
Woo-Tae Park
wtpark@seoultech.ac.kr

Citation:
Dong, C.-W., Tran, L.-G., Park, W.-T. (2021). A polymer membrane electrolysis micropump powered by a compact wireless power transmission system. Journal of Mechanical Science and Technology 35 (2) (2021) 697~706.
http://doi.org/10.1007/s12206-021-0130-2

Received July 10th, 2020
Revised September 22nd, 2020
Accepted October 22nd, 2020

† Recommended by Editor Chang-Soo Han

A polymer membrane electrolysis micropump powered by a compact wireless power transmission system

Chao-Wei Dong[1], Le-Giang Tran[2] and Woo-Tae Park[1,2]

[1]Department of Mechanical Engineering, Seoul National University of Science and Technology, Seoul, Korea, [2]Convergence Institute of Biomedical Engineering and Biomaterials, Seoul National University of Science and Technology, Seoul, Korea

Abstract In this study, a polydimethylsiloxane (PDMS) membrane electrolysis micropump activated by a miniaturized wireless power transfer (WPT) system is introduced. The micropump system has total dimensions of 20 × 14 × 8.2 mm^3. Combined with a compact WPT system, the micropump enables the delivery of drugs to the treatment area on demand. The WPT system consists of an impedance matching network and a two-stage voltage multiplier. Voltages ranging from 0.8 V to 1.3 V can be generated at different operating distance of 8 cm to 20 cm away from the RF source. The micropump is capable of delivering liquid continuously over a flow ranging from 0.11 μL/min to 4.84 μL/min. This micropump demonstrates a maximum cumulative released drug volume of up to 100.8 μL and was able to produce a pressure that is higher than the intraocular pressure. The results can be used for the study of age-related macular degeneration, diabetic retinopathy, and other ophthalmic diseases.

1. Introduction

The demand is increasing for drug delivery devices for ophthalmic treatments. The World Health Organization (WHO) estimates that at least 2.2 billion people worldwide suffer from eye impairment or loss of vision as a result of eye diseases and approximately 50 % of these people have a vision impairment that could have been prevented but has not yet been treated [1]. Among this 50 %, there are people with moderate or severe distance vision impairment or blindness due to unaddressed refractive errors (123.7 million), cataracts (65.2 million), glaucoma (6.9 million), corneal opacities (4.2 million), diabetic retinopathy (3 million), and trachoma (2 million) [2]. Drug therapy plays an important role in various biomedical applications and disease treatments [3]. Traditional drug treatments including oral swallowing, eye drops, and intravenous injections have been widely used in eye diseases treatments [4]. However, these traditional methods are limited in their therapeutic effectiveness and drug delivery efficiency. For example, most diseases are treated by eye drops or topical administration [5]. This limits the bioavailability of injectable drugs, reducing the effectiveness of drug therapy and requiring frequent administration for the long-term treatment of diseases such as diabetes retinopathy [6], which undoubtedly brings more pain and discomfort to patients. Furthermore, owing to many physical and biochemical obstacles such as the presence of the anterior tear membrane, corneal structure, and biological physiological characteristics, the bioavailability of traditional topical drug is often limited [7]. For strong drugs, the dose must be precisely controlled within the effective therapeutic concentration range, which is difficult to achieve by traditional drug delivery methods. Since the amount of a drug in the drug delivery process will gradually decrease or even fall to the level of ineffectiveness, it is necessary to design a drug delivery device that can deliver drugs quantitatively and on demand [8].

Microelectromechanical systems (MEMS) are mechatronic systems whose component's characteristic size and operating range are in the microscale. MEMS have enabled a wide range of sensors and actuators to be realized by allowing electrical devices to be placed onto

microchips [9]. With the increasing maturity of MEMS technology in recent years, flow sensors, microvalves, microfluidic chips have been intensively developed for biochemical analysis [10], drug delivery systems such as microneedles for controlled delivery, and new ophthalmic drug delivery systems (treatment for glaucoma, cataracts, etc.) have been developed in Refs. [11, 12]. MEMS-fabrication-based micropumps for microscale devices have been studied by researchers [13]. There are many types of micropumps based on a MEMS system, including drug transport devices controlled by electromagnetic fields [14, 15], artificial compression spring-driven micropump [16], and piezoelectrically actuated micropumps [17].

Unlike other MEMS-driven mechanisms, the electrolytic drive uniquely provides the following features: no moving parts, reliable operation, low energy consumption, easy manufacturing, and no maintenance. The pump mechanism is based on electrolysis. Electrolytic micropumps generally use direct current (DC) to separate electrolytes into gases. The electrolyzed gases, oxygen (O_2) and hydrogen (H_2), induce an actuation force by different pressures to drive the micropump. The drug solution in the drug reservoir is driven out of the catheter by pressure. Although the electrolytic micropump can be constructed in different ways, the pump usually consists of at least two electrodes (usually gold, palladium, or platinum) immersed in electrolyte. The electrolytic micropump has a simple structure and is simple and convenient to manufacture.

In the past 15 years, researchers have been making breakthroughs in the field of drug delivery related to implantable micropumps that were applied to rabbits and mice [18-20]. Yi et al. improved the repeatability of the electrolysis micropump by introducing a platinum (Pt)-coated carbon fiber mesh as a catalytic reforming element that can speed up the conversion of the electrolysis process. Owing to the fast gas recombination rate, the micropump cycle was improved, allowing for a shorter drug release cycle. A solid drug in the reservoir method allowed a small amount of solid drug to dissolve in the drug chamber; pulse power was used to drive the release of the drug solution [21]. Electrodes based on printed circuit boards (PCBs) are low in cost, simple to fabricate, have good electrical conductivity. Water electrolysis process is a well-known method to generate oxygen and hydrogen [22]. The micropump is moving toward miniaturization, implantability, an unlimited remote control. Batteries are no longer the first choice to reduce the size of the micropump power supply. A wireless power transfer system that continuously charges the capacitor is one energy storage method [23]. Meng et al. successfully demonstrated wireless operation utilizing inductive power transfer with a rectifier circuit at a flow rate of 3.4 μL/min [24].

In this work, we propose of using RF power to the pump wirelessly. RF wireless power has the advantage over inductive coupled wireless power because of its longer range of operation. The fabrication of the pump is done by simple PDMS fabrication techniques and PCB fabrication. The main features of the system are: (1) Powered by RF wirelessly enabling operation range up to 20 cm. (2) Reduced electrolysis pump overall size using a 2-layer PCB design. (3) Controlled the release of drug doses. In addition, the power consumption associated with this pump type was less than 1 mW. We demonstrate the feasibility of the device in terms of, delivery flow rate, cumulative delivery volume, pressure generated, and the maximum operation distance.

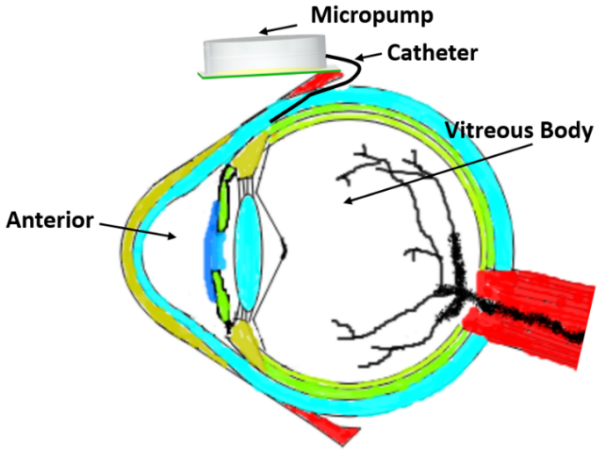

Fig. 1. Concept of the ophthalmic drug delivery micropump depicting electrolysis pumping of drug into the eye.

2. Theory and design

The electrolytic actuation method has garnered attention with its low power consumption, compact size, and the ability to produce a large displacement. As an effective means of pumping fluid, the electrolytic drive has been widely used in microfluidic devices [25, 26]. The electrolysis process was applied to drive a wireless micropump for intraocular drug delivery applications. The pressure generated by electrolysis will squeeze the drug reservoir, and the drug solution can be discharged through a flexible catheter. Drug solution is delivered to the treatment site to achieve targeted drug treatment (Fig. 1). For the treatment of human intraocular diseases, the flow rates below 2 μL/min is preferred for ocular drug delivery [19].

2.1 Electrolysis micropump module

Fig. 2 illustrates the working principle of the electrolysis micropump. The micropump is normally off until wirelessly activated by the WPT. Once the voltage is applied at the electrodes, the electrolysis process begins. The generated gas generates bubbles and this causes the pressure to increase.

The increased pressure causes the PDMS membrane to move upward, allowing the drug stored in the reservoir to be pushed out through the catheter.

There is a 1-mm-diameter round hole in the tank to allow the drug to flow out of the catheter. Because water molecules have a stable molecular structure at room temperature, the electrochemical decomposition energy of water is relatively high [27]. Under normal laboratory conditions, water molecules require a

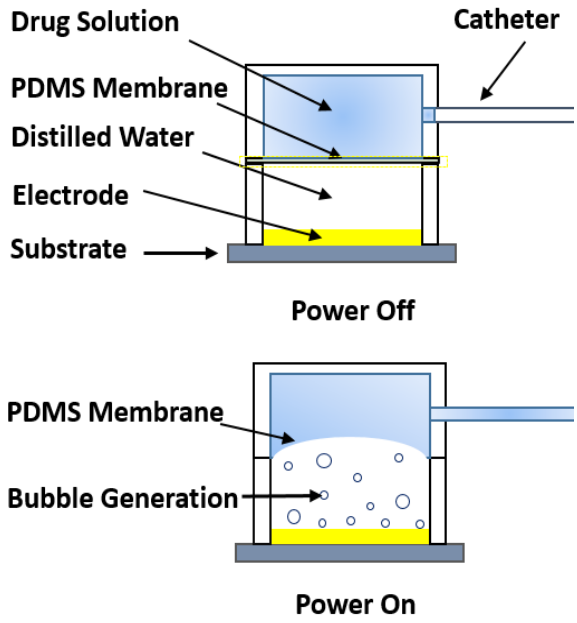

Fig. 2. Schematic diagram of the operation principle of the micropump.

minimum voltage of approximately 1.23 V to break H_2O into H_2 and O_2 [28]. It is well-known that alkali and acid or metal salts increase the ion concentration in the solution. Therefore, NaCl solution was added to the distilled water to increase the ion concentration and improve the electrolysis efficiency. In addition, Nafion® is a fluoropolymer with excellent electrical conductivity. Nafion®-coated electrode surface was used to increase the delivery flow rate and reduce electrode damage under high-voltage operation [29]. The Nafion can also improve the efficiency of bubble generation [30].

An exploded view of the electrolysis pump system is presented in Fig. 3. The micropump system was composed of an electrolysis micropump module and a WPT module located above and below a dual layer PCB. The electrolysis micropump consisted of a pair of electrodes, an enclosed pumping chamber, polymer membrane, drug reservoir, and catheter. Gold was used in the coating on the surface of the electrode to prevent the copper electrode from being oxidized.

2.2 Wireless power transmission module

A block diagram of the wireless power WPT is shown in Fig. 4 shows how the micropump works. The WPT system was based on the work previously reported [23]. An RF signal generator and panel antenna were used as a transmitting source to send RF electromagnetic waves in space. The transmitted electromagnetic signal was received by the receiving module and transmitted to the micropump. The WPT circuit included three modules: a receiving antenna, impedance matching network (IMN), and 2-stage voltage multiplier. The receiving antenna was used to receive signals. A ceramic antenna was used in the WPT circuit for their compact size. The IMN was a group of capacitors and inductor to match the impedance of the

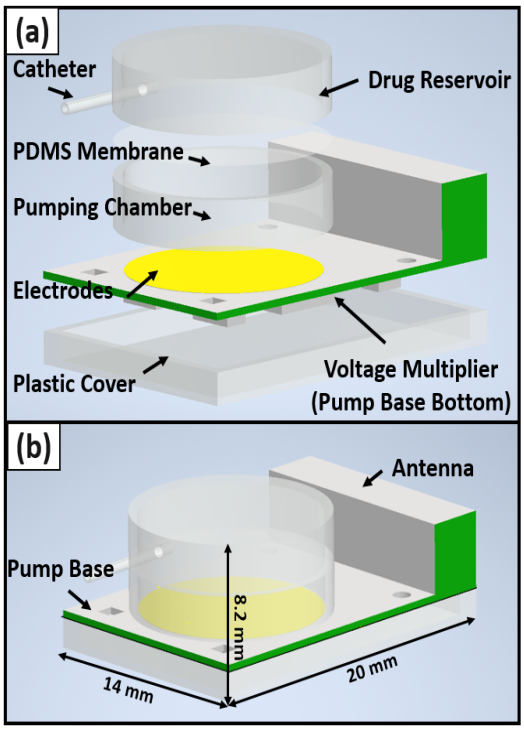

Fig. 3. Schematic design of the electrolytic micropump: (a) exploded-view diagram of the electrochemical actuator and major components; (b) assembled drug delivery system.

ceramic antenna and voltage multiplier in order to get an efficient power transmission within the circuit. The 2-stage voltage multiplier converted AC voltage into DC voltage and doubled the induced DC voltage. Here, the electrolysis electrode was considered as a load of the WPT circuit. Therefore, the electrolysis electrode was directly connected to the output of the 2-stage voltage multiplier.

3. Fabrication

The dual layer PCB was fabricated by Hansaem Digitec, Korea. The PCB was designed with two-layers (top: electrolysis electrode, bottom: WPT circuit) as shown in Fig. 5. The micropump's octagon electrodes (75 μm width, 125 μm spacing), 8 mm overall size were located on the top surface of the two-layer PCB (thickness 1.5 mm), as shown in Figs. 5(a)-(c). The electrodes were made of copper (35 μm height) and treated with the ENIG process. The outside of the electrode was covered with a gold coating (0.05 μm height), and nickel coating (7 μm height) which helps to prevent from oxidation. PDMS (SYLGARD™ 184, Dow Corning Cooperation) with a mixture of crosslinking agent at a ratio of 10:1 was used to fabricate the micropump structure. The cylinder pumping chamber and drug reservoir was built by punching a block of PDMS using a biopsy punch. The PCB was designed with two pumping chamber and drug reservoir have the same size internal diameter of 8 mm and thickness of 1 mm. It was designed to contain 150 μL of electrolyte and drug solution each, respectively.

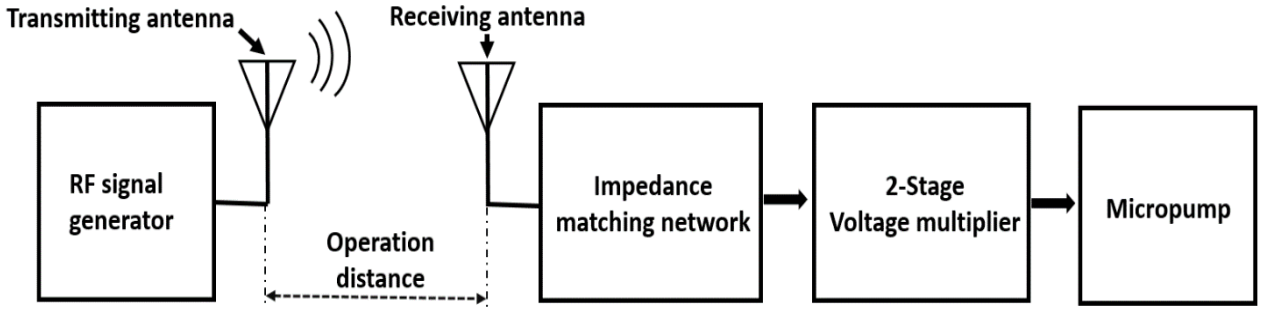

Fig. 4. Block diagram of the wireless powered electrolysis micropump system.

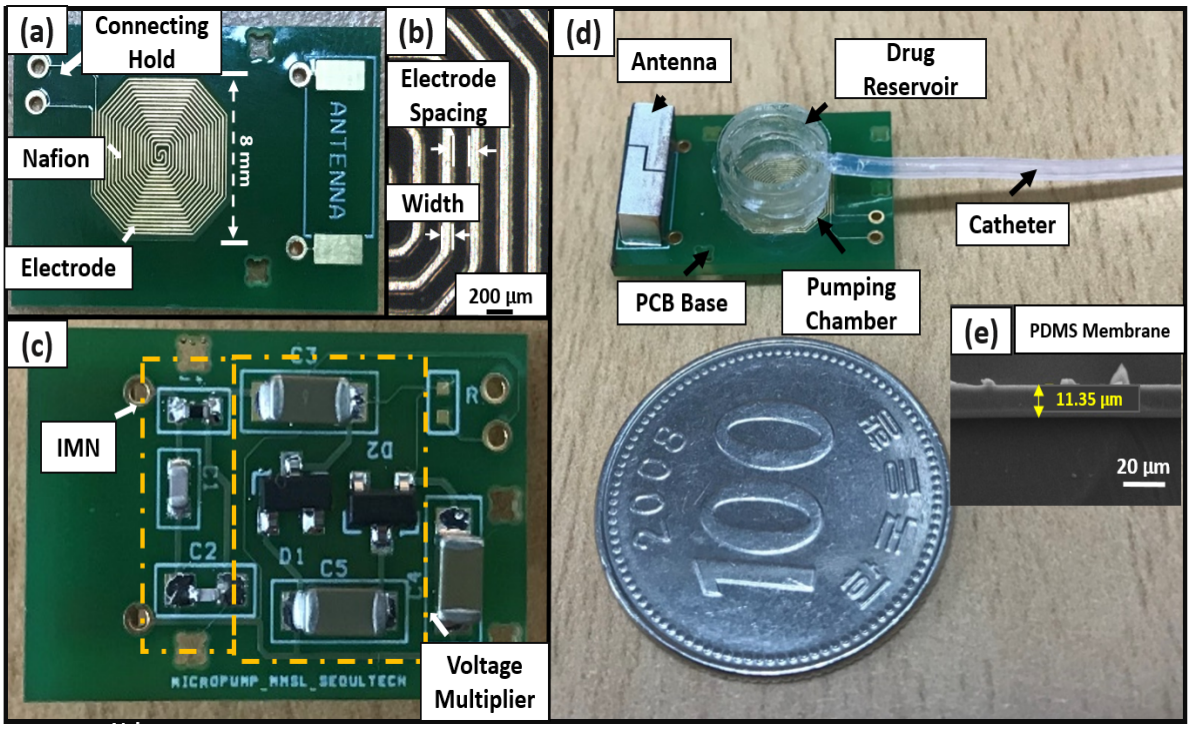

Fig. 5. Photographs of the electrolysis micropump: (a) topside PCB with ENIG electrodes in an octagon pattern; (b) close up photo of the electrodes; (c) photograph of receiving module showing IMN and voltage multiplier circuit; (d) assembled micropump system; (e) SEM image of the PDMS membrane.

PDMS membrane was fabricated by spin-coating on a Si wafer (at a speed of 5500 rpm for 30 s) using a spin-coater (ACE-200, Korea), and was finally heated at 70 °C for 2 h on a hot plate. An assembled micropump is shown in Fig. 5(d). As electrolysis process generates gases [19], it induces an actuation force that pushes a flat PDMS membrane bends upward owing to the expansion of the gas. Therefore, the thinner the membrane thickness, the more displacement of the pump given the same generated pressure. The target thickness of the PDMS membrane was around 11 μm [Fig. 5(e)]. This was the thinnest thickness of 10:1 PDMS that we could reliably fabricate with good uniformity. By setting the experimental parameters such as coating speed, and time, the thinner membrane can be fabricated. However, membranes thinner than 10 μm was difficult to peel off from the silicon wafer and easily ruptured under the operating pressure.

4. Experimental methods

4.1 Real-time electrolysis pressure & flow rate measurement

A pressure sensor and microcontroller (Arduino Uno R3, Italy) were used to measure the pressure of the pumping chamber in real-time to characterize the performance of the micropump. As shown in Fig. 6(a), a pressure sensor (WPXV5100DP, Freescale) was directly connected to the micropump catheter. The output of the pressure sensor was monitored on a laptop through the microcontroller.

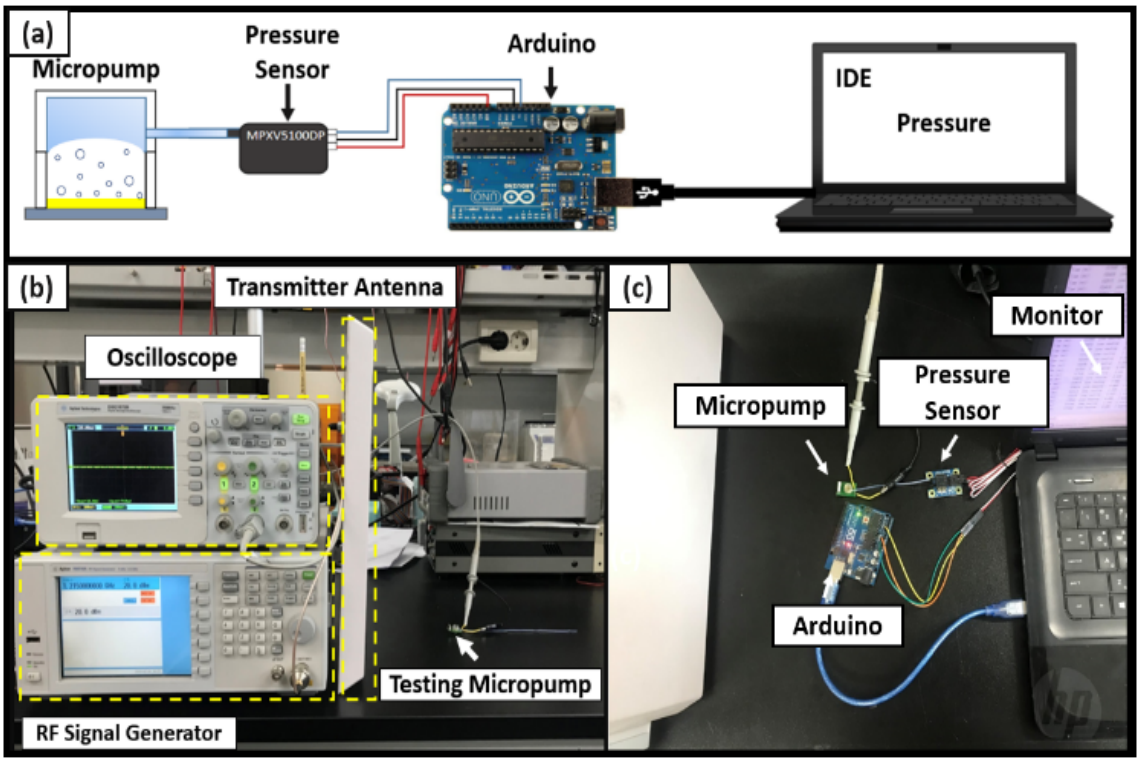

Fig. 6. (a) Schematic diagram of the pressure test setup; (b) photograph of the experimental set up to measure micropump's output flow rate; (c) close up photograph of the pressure test setup.

4.2 Wireless operation

As mentioned above, the objective of this study is to achieve wireless control of the micropump. In this experiment, distilled water was used as the main electrolyte in the pumping chamber. To increase the ion concentration and electrolyte conductivity, diluted sodium chloride 0.9 wt% NaCl solution was added into electrolyte. NaCl solution was filled into the pumping chamber and drug reservoir. The flow rate and volume of the liquid discharged from the catheter were calculated by measuring the liquid displacement in the catheter use a mitutoyo (CD-15AX, Japan) [Fig. 6(b)]. An RF signal generator (Agilent N9310A, Keysight Technologies) was used as a signal source to produce an RF signal at 1.215 GHz with a magnitude of +20 dBm. The transmitting antenna was a panel antenna ARC-PCA0913B01 (ARC Wireless LLC). To measure the voltage received by the micropump, an oscilloscope (Agilent DSO1072B) was connected in parallel to the micropump. According to the voltage measured by this oscilloscope, the total efficiency of the WPT system was calculated. There were no obstacles between the transmitting antenna and the micropump system.

5. Results

5.1 Real-time electrolysis pressure measurement

Fig. 6(c) shows the close up photograph of the pressure test setup and Fig. 7 shows the real-time pressure generated by electrolysis in the pumping chamber. The pressure increase rate was positively correlated to the applied voltage, as predicted. The pressure generated in the pumping chamber increased faster at higher input voltage. At the input voltage of 1.3 V, the generated pressure reached 1.6 kPa after 10 min, which is higher than intraocular pressure (IOP) [19]. Whereas at 1.1 V input voltage, the electrolysis pressure surpassed IOP

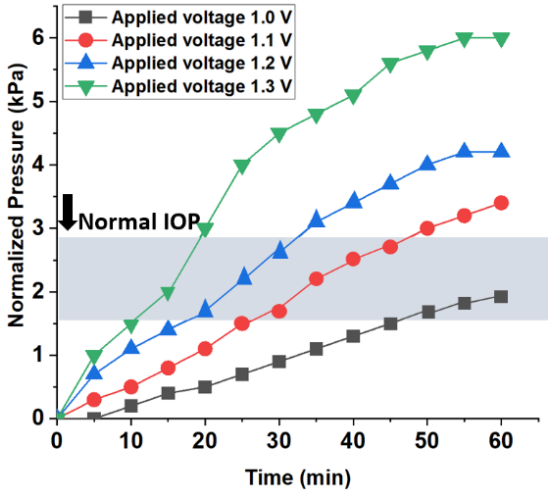

Fig. 7. The electrolysis pressure in the pumping chamber at different applied voltage.

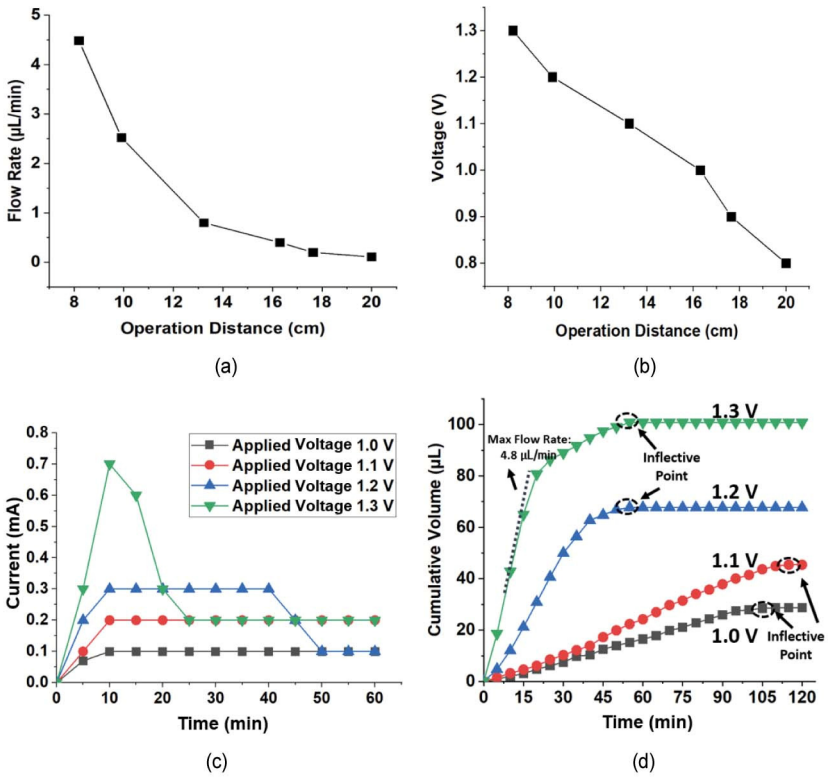

Fig. 8. Flow rates and cumulative volume testing for micropump power by WPT system: (a) performance of the micropump system under distance-controlled condition from 8 cm to 20 cm; (b) the generated voltages by WPT system at different operation distances; (c) the electrolysis currents at different voltages; (d) cumulative volume released by the micropump under supplied voltages ranging from 1.0 V to 1.3 V.

after 30 min, which was almost triple the time in the case of 1.3 V.

5.2 Flow rates and cumulative volume

The correlation between the operation distance, voltage, and the flow rate was analyze [Figs. 8(a) and (b)]. The maximum flow rate achieved was 4.84 μL/min at a supply voltage of 1.3 V and operation distance of 8 cm. The micropump obtained a flow rate ranging from 0.11 μL/min to 4.48 μL/min for an operation distance ranging from 8 to 20 cm. A minimum voltage of 0.8 V was obtained at 20 cm with a corresponding flow rate of 0.11 μL/min.

The current of the micropump was measured every 5 min during the entire experiment, as shown in Fig. 8(c). The electrolysis process was boosted by the high supply voltage (1.3 V) (0-10 min). Spontaneously, the high supply voltage facilitated the oxidation process of the electrodes. Since oxides of metals have lower conductivity than the metals themselves, this decreased the electrolysis process. Therefore, we observed a drop in the current (15-25 min) followed by a plateau in the release volume. The cumulative volume of the micropump is shown in Fig. 8(d). The micropump stopped pumping after about 55 minutes for the 1.2 and 1.3 volt condition. This indicated that the micropump reached its fluid discharge limit so the pressure did not continue to increase.

We defined the inflective point of the micropump which is the maximum cumulative volume of the micropump as a function of input voltage and operation time. In order to find the deflective point, we first calculate the cumulative volume as a function of time:

$$V = 0.84 \times \left(\frac{1}{2} \times a \times t^2 \right) \tag{1}$$

where V is the cumulative volume (μL), 0.84 is the cross-section area of the catheter (mm^2), a is the accelerated speed of the flow rate mm/s^2, and t is time (s). The deflective point is the volume when $V'' = 0$, where the cumulative volume is largest. Before the inflective point, the cumulative volume increased quickly. The flow rate reached a maximum of 4.8 μL/min (1.3 V supply voltage) after 10 min. After the inflective point, the flow rate gradually decreased until it reached a maximum cumulative volume of 100.8 μL. When the micropump was supplied by a small voltage (< 1.2 V), the flow rate was more stable. The inflective points of the supplied voltages of 1.0 V and 1.1 V appeared, respectively, at 105 min and 115 min at minimum flow rates of 0.14 μL/min and 0.11 μL/min. In general, the deflective point informed the maximum drug volume that a micropump can achieve under certain conditions. It may be desirable to match the deflective point to the specific

drug dose in real applications.

5.3 Pump efficiency

As mentioned above, the actuation force of the electrolysis micropump comes from the separation of water into hydrogen and oxygen. The electrolysis of water was selected as the actuation mechanism for low power consumption, high pump efficiency, simple structure, and the ability to generate large displacements [31, 32]. The corresponding electrochemical reactions are given by

Anode: $2H_2O(l) \leftrightharpoons O_2(g) + 4H^+(aq) + 4e^-$
Cathode: $2H_2O(l) + 2e^- \leftrightharpoons 2OH^-(aq) + H_2(g)$
Net: $2H_2O(l) \leftrightharpoons O_2(g) + 2H_2(g)$

The electrolysis discrepancy (η) of water can be defined as

$$\eta = \frac{V_{experimental}}{V_{theoretical}} \tag{2}$$

where $V_{experimental}$ is the generated gas volume by measurements, and $V_{theoretical}$ is the theoretical volume of the generated gas [33]. $V_{theoretical}$ is closely related to the applied current [34]. The corresponding theoretical generated volume can be calculated by

$$q_{theoretical} = \frac{3}{4} \times \frac{i}{F} \times V_m \tag{3}$$

where i is the current in amperes, F represents Faraday's constant (96.49 × 10^3 C/mol), and V_m is the atmospheric pressure (24.7 × 10^{-3} m^3/ mol) at room temperature. If obtained current is used, $V_{theoretical}$ can be calculated as

$$V_{theoretical} = q_{theoretical} \times t \tag{4}$$

where $V_{theoretical}$ is the theoretical gas generation rate (m^3/s) and t is the electrolytic time in seconds. We assumed that the volume of the discharged drug in the reservoir was proportional to the generated gas ($V_{theoretical}$) in the pumping chamber. Therefore, the pump efficiency can be calculated by taking ratio of the applied voltage to the output flow rate as shown in Fig. 9.

$$\eta_{pump} = \frac{Applied\ voltage}{Flow\ rate}. \tag{5}$$

The micropump achieved maximum efficiency of 80.6 % at the applied voltage of 1.3 V. The efficiency dropped to 51.2 % and 50.0 % at the applied voltage of 1.2 V and 1.1 V, respectively. Additionally, we noticed that there is a trade-off between efficiency and sustainability of the electrolysis micropump. At the supplied voltage of 1.3 V, the generated flow rate was up to 4.84 μL/min [Fig. 8(a)], however this high flow rate quickly dropped to null as electrodes were oxidized. On the other hand, the oxidation reaction was observed to be negligible at low applied voltages whereas the electrolysis efficiency as around less than or equal 50 %. Therefore, the flow rates remained stable for a long period of time, which were up to 2 h [Fig. 8(d)] for the micropump efficiency of 40 % and 50 % (Fig. 9).

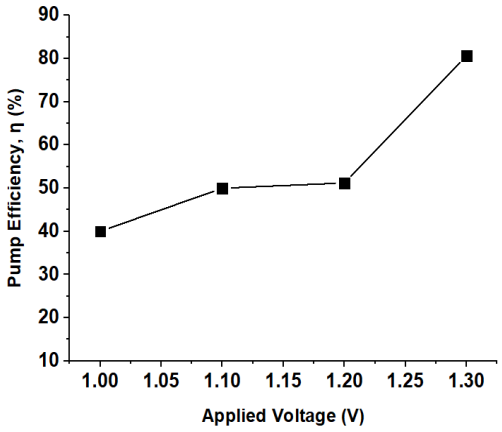

Fig. 9. Micropump efficiency optimization based on applied voltage.

5.4 Total efficiency of WPT system

An important parameter to evaluate the performance of the WPT system is the total efficiency η_e. By calculating and analyzing the efficiency η_e, the circuit design of the micropump driver can be guided and optimized to reduce unnecessary power consumption. The η_e of the system is calculated as

$$\eta_e = \frac{P_{DC}}{P_{in}} = I \times V \times \frac{1}{P_{in}} \tag{6}$$

where P_{DC} is the output measured power consumed by the micropump, I is the current, V is the applied voltage, and P_{in} is the RF power emitted by the transmission antenna. Here we assumed that the power harvested by the WPT was fully transmitted to the micropump. Using Eq. (6), the total efficiency of the WPT system was calculated, and the result is shown in Fig. 10. The low η_e of the WPT system was expected due to the high transmission loss of electromagnetic wave in space. Additionally, the small size of the receiving antenna which was used in the micropump system made it receive less electromagnetic power. The highest η_e was 0.91 % which was achieved at a distance of 8 cm from the source. The ηe rapidly reduced as the micropump system was shifted away from the source, down to 0.05 % at 20 cm away from the source. Though the WPT system achieved less than 1 % η_e, it produced sufficient power to drive the micropump.

6. Discussion

In this study, we developed a wireless electrolysis micro-

Table 1. A comparison between this work and other micropump designs.

Ref.	Source of energy	Size (mm)	Electrodes	Max. operation distance (cm)	Max. power consumption	Transmission frequency	Max. flow rate (μL/min)
[20]	Inductive powering	20×15×8	Ti/Pt	4	1 mW	2 MHz	~3.30
[24]	Inductive powering	NA	Ti/Pt	NA	~ 0.4 mW	200 MHz	3.40
[35]	Ultrasonic transducer	22×7×5	Pt	11	~ 9 mW	1.15 MHz	0.23
[36]	RF magnetic	Diameter: 10 Height: 5	Cu	NA	5 W	153 MHz	0.17
[37]	Inductive powering	NA	Pt	5	0.36 mW	500 kHz	1.04
This work	Miniature WPT system	20×14×8.2	Cu	20	0.9 mW	1.215 GHz	4.84

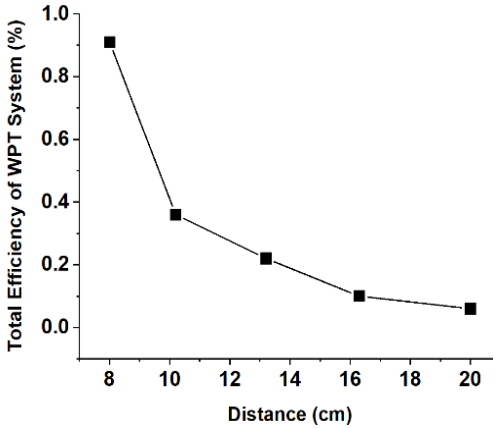

Fig. 10. The total efficiency of the WPT system versus distance between transmitting antenna and WPT system.

pump that able to deliver the drug at a maximum flow rate of 4.84 μL/min. The electrolysis micropump is easy to manufacture and simple to use. The micropump is designed to store up to 150 μL of the drug solution in a reservoir to meet the treatment demand. The micropump can discharge 100.8 μL of drug solution, accounting for 66.7 % of the drug reservoir. This reduces any wasted drugs owing to dead volume. We optimized the design of the WPT module to greatly reduce the overall size and weight of the micropump system. The micropump can be operated wirelessly at the maximum operation distance of 20 cm, thus increasing the space flexibility of the micropump.

A comparison of the specifications of the micropump to those of related studies is shown in Table 1. The micropump provides a wide range of flow rates. The drug release flow rate was ranging from 0.11 μL/min to 4.84 μL/min when the operation distance was adjusted from 8 to 20 cm. The WPT system offers longer operation distance than other inductive powering systems [20, 24], ultrasonic powering system [35], and integrated implantable electrolytic micropump [37]. Cobo et al. demonstrated a wireless infusion micropump that uses an inductive power system to drive the micropump for chronic drug delivery in small animals [20], with an average flow rate of 3.3 μL/min. The ultrasound-driven implantable micropump can reach the flow rate of 0.23 μL/min at 11 cm operation distance [35] while our electrolysis micropump was able to obtain the similar flow rate at 18 cm operation distance.

Additionally, the wireless electrolysis micropump developed produce a high range of flow rate for a variety of applications. The micropump achieved a high flow rate (4.84 μL/min) while consuming less power than other presented micropumps [20, 35, 36]. Note that the maximum flow rate was compared in wireless operation mode only. As for intraocular drug delivery, the required flow rate was no more than 2 μL/min [19], our micropump can induce sufficient flow rate for intraocular drug delivery from a distance of 10 cm.

On the other hand, we noticed the oxidation of the electrode during the electrolysis process especially at high operation voltage (1.3 V). Even though the electrode was treated with ENIG process, it was not able to protect the electrode against high voltage for a long time. Therefore, the electrode needs further optimization to prevent it from oxidation. Additionally, the drug solution was replaced with distilled water in the experiment, and thus the flow rate may be different from the actual supply of the drug solution. Extensive animal studies are needed and planned to comprehensively assess the pharmacological efficacy and safety of these areas.

7. Conclusion

A fully wireless electrolysis micropump system was fabricated and demonstrated. The micropump system induced flow rates ranged from 0.11 μL/min to 4.84 μL/min with an operation distance up to 20 cm. The micropump efficiency was 80.6 % and the actuation pressure was up to 6 kPa, which is higher than the intraocular pressure. This indicates that the wireless electrolysis micropump system can be used for ophthalmic drug delivery. The micropump system was designed to be compact and light-weight with simple fabrication process. The targeted application of this study was the administration of eye drug treatments but can be applied to other drug delivery applications as well.

Acknowledgments

This research was sponsored by the Seoul National Univer-

sity of Science and Technology Internal Research Fund (2019-0497).

References

[1] WHO, *Blindness and Vision Impairment*, The World Health Organization (2019).

[2] T. R. Fricke et al., Global prevalence of presbyopia and vision impairment from uncorrected presbyopia: systematic review, meta-analysis, and modelling, *Ophthalmology*, 125 (10) (2018) 1492-1499.

[3] Y. Yi, A remotely powered electrolytic actuator with dose control for implantable drug delivery, *Doctor's Thesis*, The University of British Colombia (2016).

[4] S. Z. Razzacki, P. K. Thwar, M. Yang, V. M. Ugaz and M. A. Burns, Integrated microsystems for controlled drug delivery, *Adv. Drug Deliv. Rev.*, 56 (2) (2004) 185-198.

[5] R. R. Joseph and S. S. Venkatraman, Drug delivery to the eye: what benefits do nanocarriers offer?, *Nanomedicine*, 12 (6) (2017) 683-702.

[6] C. Di Tommaso et al., Novel micelle carriers for cyclosporin A topical ocular delivery: in vivo cornea penetration, ocular distribution and efficacy studies, *Eur. J. Pharm. Biopharm.*, 81 (2) (2012) 257-264.

[7] S. Awwad et al., Principles of pharmacology in the eye, *Br. J. Pharmacol.*, 174 (23) (2017) 4205-4223.

[8] E. Meng and T. Hoang, MEMS-enabled implantable drug infusion pumps for laboratory animal research, preclinical, and clinical applications, *Adv. Drug Deliv. Rev.*, 64 (14) (2012) 1628-1638.

[9] W. C. Chuang, H. L. Lee, P. Z. Chang and Y. C. Hu, Review on the modeling of electrostatic MEMS, *Sensors*, 10 (6) (2010) 6149-6171.

[10] X. Ou, P. Chen, X. Huang, S. Li and B. Liu, Microfluidic chip electrophoresis for biochemical analysis, *Journal of Separation Science*, 43 (1) (2019) 1-55.

[11] P. Singh et al., Polymeric microneedles for controlled transdermal drug delivery, *J. Control. Release*, 315 (2019) 97-113.

[12] O. Cegielska and P. Sajkiewicz, Targeted drug delivery systems for the treatment of glaucoma: most advanced systems review, *Polymers (Basel)*, 11 (11) (2019).

[13] M. W. Ashraf, S. Tayyaba and N. Afzulpurkar, Micro electromechanical systems (MEMS) based microfluidic devices for biomedical applications, *Int. J. Mol. Sci.*, 12 (6) (2011) 3648-3704.

[14] Y. Yi, A. Zaher, O. Yassine, J. Kosel and I. G. Foulds, A remotely operated drug delivery system with an electrolytic pump and a thermo-responsive valve, *Biomicrofluidics*, 9 (5) (2015) 1-9.

[15] C. Wang et al., Intravitreal implantable magnetic micropump for on-demand VEGFR-targeted drug delivery, *J. Control. Release*, 283 (2018) 105-112.

[16] X. Zhang, K. Xia, A. Ji and N. Xiang, A smart and portable micropump for stable liquid delivery, *Electrophoresis*, 40 (6) (2019) 865-872.

[17] G. H. Feng and E. S. Kim, Piezoelectrically actuated dome-shaped diaphragm micropump, *J. Microelectromechanical Syst.*, 14 (2) (2005) 192-199.

[18] S. Saati, R. Lo, P. Y. Li, E. Meng, R. Varma and M. S. Humayun, Mini drug pump for ophthalmic use, *Curr. Eye Res.*, 35 (3) (2010) 192-201.

[19] P. Y. Li et al., An electrochemical intraocular drug delivery device, *Sensors Actuators, A Phys.*, 143 (1) (2008) 41-48.

[20] A. Cobo, R. Sheybani, H. Tu and E. Meng, A wireless implantable micropump for chronic drug infusion against cancer, *Sensors Actuators, A Phys.*, 239 (2016) 18-25.

[21] Y. Yi, U. Buttner and I. G. Foulds, A cyclically actuated electrolytic drug delivery device, *Lab Chip*, 15 (17) (2015) 3540-3548.

[22] D. N. Pagonis, A. Petropoulos and G. Kaltsas, A pumping actuator implemented on a PCB substrate by employing water electrolysis, *Microelectron. Eng.*, 95 (2012) 65-70.

[23] L. G. Tran, H. K. Cha and W. T. Park, A compact wireless power transfer system at 915 MHz with supercapacitor for optogenetics applications, *Sensors Actuators, A Phys.*, 285 (2019) 386-394.

[24] P. Y. Li, R. Sheybani, C. A. Gutierrez, J. T. W. Kuo and E. Meng, A parylene bellows electrochemical actuator, *J. Microelectromechanical Syst.*, 19 (1) (2010) 215-228.

[25] C. Szydzik et al., Active micropump-mixer for rapid antiplatelet drug screening in whole blood, *Anal. Chem.*, 91 (16) (2019) 10830-10839.

[26] H. Fallahi, J. Zhang, H. P. Phan and N. T. Nguyen, Flexible microfluidics: fundamentals, recent developments, and applications, *Micromachines*, 10 (12) (2019).

[27] F. N. Lin and S. W. Walker, Economics of liquid hydrogen from water electrolysis, *International Journal of Hydrogen Energy*, 10 (12) (1985) 525.

[28] K. Mazloomi, N. Sulaiman and H. Moayedi, Electrical efficiency of electrolytic hydrogen production, *International Journal of Electrochemical Science*, 7 (4) (2012) 3314-3326.

[29] R. Sheybani and E. Meng, High-efficiency MEMS electrochemical actuators and electrochemical impedance spectroscopy characterization, *J. Microelectromechanical Syst.*, 21 (5) (2012) 1197-1208.

[30] Y. Yi, U. Buttner, A. A. A. Carreno, D. Conchouso and I. G. Foulds, A pulsed mode electrolytic drug delivery device, *J. Micromechanics Microengineering*, 25 (10) (2015) 105011.

[31] C. Neagu, H. Jansen, H. Gardeniers and M. Elwenspoek, Electrolysis of water: an actuation principle for MEMS with a big opportunity, *Mechatronics*, 10 (4) (2000) 571-581.

[32] C. R. Neagu, J. G. E. Gardeniers, M. Elwenspoek and J. J. Kelly, An electrochemical microactuator: principle and first results, *J. Microelectromechanical Syst.*, 5 (1) (1996) 2-9.

[33] J. Xie et al., An electrochemical pumping system for on-chip gradient generation, *Anal. Chem.*, 76 (13) (2004) 3756-3763.

[34] C. A. Paddon et al., Towards paired and coupled electrode reactions for clean organic microreactor electrosyntheses, *J. Appl. Electrochem.*, 36 (6) (2006) 617-634.

[35] J. Zhou, A. Kim, M. Ochoa, H. Jiang and B. Ziaie, An ultrasonically powered micropump for on-demand in-situ drug delivery, *Proc. IEEE Int. Conf. Micro Electro Mech. Syst.* (2016) 349-352.
[36] M. A. Zainal, A. Ahmad and M. S. Mohamed Ali, Frequency-controlled wireless shape memory polymer microactuator for drug delivery application, *Biomed. Microdevices*, 19 (1) (2017) 1-10.
[37] R. Sheybani, A. Cobo and E. Meng, Wireless programmable electrochemical drug delivery micropump with fully integrated electrochemical dosing sensors, *Biomed. Microdevices*, 17 (4) (2015) 1-13.

Chao-Wei Dong received his B.S. degree in Mechanical Engineering from Hannam University, Korea, in 2019. He is currently working toward the M.S. degree in Mechanical Engineering Department of Seoul National University of Science and Technology. His research includes the characterization of electrolysis micropump and hollow microneedle for drug delivery systems.

Le-Giang Tran received his B.S. degree in Biomedical Engineering from HCMC International University, Vietnam in 2014 and M.S. degree in Biomedical Engineering and Biomaterials from Seoul National University of Science and Technology in 2016. For his M.S. research, he worked on developing a wireless power transfer system for biomedical applications. He is currently pursuing Ph.D. degree in Seoul National University of Science and Technology and is focusing on flow sensor for unmanned underwater vehicles and microneedles for intradermal drug delivery.

Woo-Tae Park received the B.S. degree in Mechanical Design from Sungkyunkwan University, Korea, in 2000, the M.S. and Ph.D. degrees in Mechanical Engineering from Stanford University in 2002 and 2006, respectively. For his Ph.D., he worked on wafer scale encapsulated MEMS devices for biomedical applications. After graduation, he worked at Intel Corporation, Freescale Semiconductor, and IME Singapore, leading several projects on MEMS development. He has authored more than 80 journals and refereed conference papers and has 14 issued and pending patents. He is currently an Associate Professor at Seoul National University of Science and Technology, conducting research on microscale medical devices.